Journal of Basic Physical Research ISSN: 2141-8403 Prints, 2141-8411 Online
Vol.12, Issue 2, October, 2024, pp. 61 - 76. Available online at https://journals.unizik.edu.ng/jbpr/

OPTIMIZING THE CONDUCTIVITY OF TITANIUM DIOXIDE IN A DYE SENSITIZED SOLAR CELL THROUGH SENSITIZER AGEING.

K. P. Alor [a*], B. A. Ezekoye [b], P. E. Ugwuoke [b], S. U. Offiah [b,c] ,K.O. Suleman[d], R. Akwolu[b], A.O. Ikenga[a] , and I.U. Chibuogwu[a]
[a] Department of Physics and Industrial Physics, Nnamdi Azikiwe University, Awka, Nigeria.
[b] Department of Physics and Astronomy, University of Nigeria Nsukka, Nigeria.
[c] National Centre for Energy Research and Development, University of Nigeria, Nsukka, Nigeria.
[d]Department of Science Laboratory Technology, Akanu Ibiam Federal Polytechnic Unwana, Afikpo, Ebonyi State, Nigeria.
*Corresponding author * Email; kp.alor@unizik.edu.ng*

Abstract
The increasing global need for energy and the depletion of fossil fuel reserves necessitate the development of clean alternative energy sources. Among the approaches for harnessing solar energy and converting it into electricity, the dye-sensitized solar cell (DSSC) represents one of the most promising methods for future large-scale power production from renewable energy sources. In these cells, the sensitizer is one of the key components, harvesting the solar radiation and converting it into electric current. The electrochemical, photo physical, and molecular electronic properties of the sensitizer play an important role for charge transfer dynamics at the semiconductor interface. The use of expensive ruthenium metals, derived from scarce natural resources for dye sensitized solar cells fabrication corresponds to a relatively heavy environmental burden, hence the necessity to use natural dyes as alternative sensitizers with appreciable efficiencies. In this researched paper, some natural dye samples were used in DSSC fabrication. The dye samples were tested using ageing technique for improved cell performance. The UV-Vis analysis proved that the aged samples has improved absorbance in the visible and near infra-red regions which are demonstrated in the photovoltaic properties. The fabricated solar cells sensitized with the aged dyes showed enhanced open-circuit voltage and efficiency.
Keywords*: Natural dyes, Ageing, Doping, Fabrication, Power conversion efficiency.*

Introduction

Solar energy has gained significant attention as a clean alternative to fossil fuels due to its renewable and abundant nature. It is considered a favored option worldwide (Bera *et al.*, 2021). Solar cells, which are semiconductor devices, are used to harness the power from the sun and convert sunlight into electricity. Solar cells are categorized into different generations based on their composition and production techniques. First-generation solar cells consist of wafer-based structures made of single crystalline silicon. These cells have a low intrinsic absorptivity, so they require thick crystals (around 300 μm) to achieve high absorption and charge carrier density (Jing *et al.*, 2022). However, achieving such large diffusion lengths requires extreme material purity, this makes the production of high-purity silicon crystals expensive. Second-generation solar cells are thin-film-based and offer alternative materials and manufacturing methods. Though numerous attempts have been devoted to further reducing the film thickness, thus far, they were not successful due to high recombination in the lower size domains (Pastuszak & Węgierek, 2022). To overcome this recombination rate, multiple layers of thin-film semiconductors with different bandgaps were often stacked to widen the absorbed wavelength range.

However, the stacking process can lead to lattice mismatch and defects which can affect the performance of the solar cells (Lai *et al.*, 2022). Third-generation solar cells are sensitizer-based and employ sensitizer materials to enhance their performance (Akwolu *et al.*, 2023). Dye-sensitized solar cells (DSSCs) are electrical devices that convert light photons into electricity through the photovoltaic effect. DSSC technology is inspired by the concept of artificial photosynthesis, which aims to replicate the ability of plants to convert sunlight into useful energy. Various metal complexes and organic dyes have been synthesized for DSSCs.

Among them, ruthenium-based (Ru) complex sensitizers have been widely used due to their better efficiency and high durability compared to other sensitizers. However, these advantages are offset by their high cost, complicated synthetic routes, and tendency to undergo degradation in the presence of water (Zhang *et al.*, 2008). An alternative approach to sourcing dyes for DSSCs is to extract them from natural sources. This provides a cheaper and abundant source of dyes while also reducing environmental pollution (Geetha & Sumathy, 2013).

A typical dye-sensitized solar cell (DSSC) consists of several components, including a transparent conductive oxide (TCO), semiconducting oxide, a photosensitizer (dye), an electrolyte, and a counter electrode. Conventional semiconducting oxide material in DSSC, titanium dioxide (TiO_2), can be modified through element doping. The photosensitizer, which is a molecule that enables chemical changes to occur in a photochemical process, plays a crucial role in determining the overall efficiency of the DSSC (Rosana & Amarnath, 2014). Traditionally, ruthenium-based dyes have been used as photosensitizers in DSSCs. However, natural dyes are being explored as alternative photosensitizers to reduce reliance on expensive ruthenium metal, which is derived from relatively scarce natural resources (Shelke *et al.*, 2013). Natural dyes are classified into different categories based on their sources of origin, such as plant, animal, mineral, and microbial dyes. Examples of environmentally friendly natural dyes include flavonoids, chlorophyll, carotenoids, tannins, and betalains (Rosana & Amarnath, 2014). There has been a growing interest in natural dyes for DSSCs due to their high availability, complete biodegradability, low cost, and ease of extraction without requiring complex synthetic procedures.

Several studies have investigated the performance of DSSCs using natural dye extracts and dopants. For example, dye pigments were extracted from natural dyes for solar cell fabrication, the result showed absorption in the visible light region, with power conversion efficiencies ranging from 0.13% to 0.48% (Onah *et al.*, 2020). Offiah *et al.*, (2021) demonstrated the performance of a DSSC based on *baphia nitida* (camwood) dye, strong absorption in the visible light region and a power conversion efficiency of 1.2 was recorded. Natural dyes extracted from fresh and dried raw materials were influenced by the drying process temperature and the dye adsorption time duration (Taya *et al.*, 2013). Different natural dyes showed varying performance in DSSCs (El-Ghamri *et al.*, 2014). Nirmala *et al.*, (2020) fabricated a DSSC using natural extracts as photosensitizers and recorded power conversion efficiencies of 0.75% and 0.40% from beetroot and turmeric respectively. El-Ghamri *et al.*, (2014), compared the efficiencies of dye sensitized solar cells fabricated with TiO_2 and ZnO photoanodes using natural dyes extracted from plant seeds. The TiO_2 photoanode gave overall best results. The impact of different dye extracting solvents and sensitizer adsorption time on the photovoltaic performance of turmeric natural sensitizer showed that dry turmeric dye has improved cell performance compared to other sources of turmeric dye, and ethanol solvent exhibited a good photovoltaic response among all the solvents used in the study (Hossain *et al.*, 2018). When different dyes are mixed, light absorbance is improved as well as the solar cell efficiency compared to using a single dye (Widhiyanuriyawan *et al.*, 2022). Syafinar *et al.*, (2015) investigated the potential of natural dyes extracted by the ultrasonic extraction method for DSSC fabrication. The results suggests that the combination of dyes has good potential for future DSSC development. García-Salinas & Ariza, (2019) optimized a simple method for producing natural dyes for dye-sensitized solar cells using different extraction methods. The fabricated dyes showed different absorption peaks at different wavelengths. Bensaha & Bensouyad, (2012) fabricated zirconium doped TiO_2 through sol-gel process, addition of ZrO_2 formed nanoparticle of anatase grain size and showed transparency in the visible range as well as decreased energy band gap for the ZrO_2-doped nanoparticle.

Synthesis of pure and doped TiO_2 nano-materials with different Zr^{4+} ions content by sol-gel method recorded a photo conversion efficiency of 8.63 % at the introduction 3.7 % Zr^{4+} ions into the TiO_2 (Bartkowiak *et al.*, 2021). Pawar *et al.*, (2019) prepared TiO_2, ZrO_2 and layer-by-layer TiO_2–ZrO_2 films. The average values of power conversion efficiencies of the DSSCs fabricated with TiO_2, ZrO_2 and layer-by-layer TiO_2–ZrO_2 photoanodes were found to be 0.65 %, 3.04 % and 3.13 %, respectively. Comparison of the cell performance of a binary TiO_2-ZrO_2 oxide and single TiO_2 photo electrodes doped TiO_2 was investigated, results showed an improved solar energy conversion efficiency with the binary TiO_2-ZrO_2 oxide. The electron life time was also observed to be prolonged from 0.63 minutes (TiO_2) to 0.91 minutes (Ti-Zr) (Waghmare *et al.*, 2019). Mohamed *et al.*, (2016) recorded cell improvement from 1.61 % to 4.52 % on solar cell fabricated with ZrO_2 dopant, sensitized with N719 dye. Another report on fabricated DSSC based on same ZrO_2 dopant but with a natural sensitizer recorded 0.23 % power conversion efficiency (Win *et al.*, 2015). Tomar *et al.*, (2016) reported an improvement in efficiency of DSSC using TiO_2-ZrO_2 and Zn-doped photoanodes. The research by Lai *et al.*,(2022) revealed that for mixed titanium-zirconium oxide system in DSSC, the open circuit voltage (V_{oc}) of the device enhanced with increase in zirconium percentage. And for higher zirconium content, the device conversion efficiency decreased drastically due to reduced electron injection. The investigation of the absorption effects, light harvesting and light scattering properties of Zr-doped TiO_2 comprising of a mixture of 0.025 wt % carbon nanotubes with TiO_2 nanoparticles, 0.025 mol % Zr doped TiO_2 nanoparticles as an over layer and 0.025 mol % Zr doped TiO_2 nanoparticles as an under layer recorded an improved power conversion efficiency of 8.19 % (Moradzaman *et al.*, 2015).

Kitiyanan *et al.*, (2005) prepared TiO_2-ZrO_2 (95 % TiO_2 + 5 % ZrO_2) mixed oxide system to increase efficiency of the cell. The cell parameters V_{oc} of the device enhanced to ~ 4 %, J_{sc} to ~ 11 % and η to ~ 17 % in comparison to a device fabricated using TiO_2 photo –electrode film. Dye-sensitized solar cells have many components that have to be optimized, both individually and then again as a component of a highly interactive assembly. In view of this, the study aimed to investigate the effect of element doping and sensitizer ageing on performance of a DSSC device.

Materials and methods

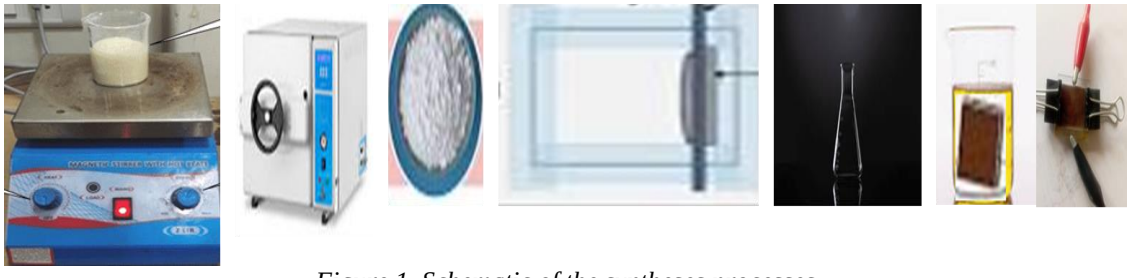


Figure 1. Schematic of the syntheses processes

Some of the materials and chemicals used includes, Teflon-lined steel autoclave, fluorine-doped tin oxide (FTO) substrates, oven, magnetic stirrer, filter papers, measuring cylinders, hand gloves, black storage bottles, titanium isopropoxide (TTIP), acetone, distilled water, zirconium nitrate ($ZrO(NO_3)_2$), absolute ethanol, acetic acid, iodide/tri-iodide ($I^-|I_3^-$) electrolyte, ethyl cellulose, terpineol.

Obtaining Natural Dye Sources

To obtain natural dye sources from the immediate environment, the items collected were fresh beta vulgaris (beetroot) and fresh curcuma longa (turmeric). These sources were then subjected to a washing process using clean water to remove any impurities.

Dye Extraction Process

The dye materials were divided into two quantities for further processing. The first set of dye sources was chopped and soaked in a beaker containing 40 ml of absolute ethanol. This mixture was then kept in a dark environment for one week to allow for extraction. After one week, the extracts were filtered, and the filtrate was aged in the dark for fourteen months before characterizations. The second set of dye materials underwent a similar extraction process. After one week of soaking, the extracts were filtered and characterized immediately without the ageing process.

Synthesis of the Photoanode for DSSC Device

The photoanode for the DSSC device was synthesized using a titanium isopropoxide (TTIP) precursor. A solution was prepared by dissolving 4 ml of TTIP in 80 ml of acetone, which was then stirred for 1 hour. The solvothermal process was carried out by transferring the solution into a Teflon-lined steel autoclave. The Teflon was placed in an autoclave at 200°C for 3 hours. After the process, the autoclave was allowed to cool, and the solution was poured into a beaker. The solution was then washed with acetone and dried at 100°C. The dried flakes were subsequently annealed at 450°C for 1 hour before being ground into a powder form. The zirconium doping followed the same procedure of synthesis using 3.88 ml of TTIP and 0.09 g of zirconium nitrate in 80 ml of acetone.

Preparation of TiO_2 Paste

To prepare the TiO_2 pastes, 0.2 g of the prepared TiO_2 powder was mixed with 0.10 g of ethyl cellulose, 0.4 ml of terpineol, and 3 ml of acetic acid (added dropwise). The mixture was ground until a homogenous mixture was obtained to the desired viscosity.

Coating the FTO Glass

The FTO (Fluorine-doped Tin Oxide) glasses were washed with absolute ethanol and left to dry. With the FTO conductive side facing up, two parallel stripes of scotch tape were applied to the edges of the conducting glass plate. The TiO_2 paste was then deposited onto the FTO glass between the two pieces of tape using the doctor blade method. This process was repeated until a homogenous layer was achieved. The film was dried at room temperature, and the tape was subsequently removed. The prepared TiO_2 film was further dried at 100°C for 1 hour and annealed at 450°C for another 1 hour. After the annealing process, the films were allowed to cool naturally.

Dye Sensitization and DSSC Assembly

The coated FTO glass, after staining with the different sets of dye extracts, were immediately rinsed with ethanol to remove any dye molecules that were not anchored on the film surface. These were then used for the assembly of the DSSCs. This process ensured the adsorption of the natural dye sources onto the solar cells.

Results and Discussions

XRD Analysis: The crystal structures of the synthesized nanoparticles were analyzed by X-ray Diffraction using Kα radiation (λ= 1.54184 Å) operating at a tube current of 40 mA and a

voltage of 40 kV. Data were recorded in a 2θ range of 10° - 70°. Figures 2 depicts the XRD patterns of the un-doped titanium and zirconium-doped titanium for the synthesized nanoparticles. From the un-doped sample, a sharp peak was observed at 25.19º, indicating its preferred growth orientation. Other smaller peaks were observed at 38.93º, 48.99º, 55.61 º and 63.64 º respectively. The synthesized zirconium-doped titanium nanoparticles recorded peak values at 24.94º, 37.68º, 47.75º, 54.35º and 62.06 º respectively. The observed peaks were indexed to the planes (101), (112), (200), 105), (204) and (116) which represent the anatase phase in the synthesized nanoparticles. The presence of these diffraction peaks endorses cubic crystal planes of anatase TiO_2 corresponding to the JCPDS Card no 21-1272 (Dubey *et al.*, 2021). A slight deviation to the left of the diffraction peaks of all the planes was noticed on the doped sample as depicted in figure 2, this indicates the substitution of the ions in the TiO_2 lattice. Such similar left shift has also been reported upon doping in the literatures (Dubey *et al.*, 2021; Mansour *et al.*, 2019). These slight deviation could be ascribed to the expansion of the TiO_2 unit cell due to the incorporation of the dopant (Nguyen & Bar k, 2020). Furthermore, a change in full width at half maxima (FWHM) of (101) peak was observed, this shows the modification in the local structures around Ti^{4+} upon doping and confirms the successful incorporation of the dopant material into the TiO_2 lattice. The dominant sharp peak and the fewer peaks present in the samples indicate that the synthesized nanoparticles were highly crystalline, and that the crystallinity improved on doping (Dubey *et al.*, 2021). Considering the dominant peak of the plane (101) at angle 2θ, as noticed for the synthesized nanoparticles, the crystallite size was estimated using Debye-Scherrer formula. The obtained crystallite sizes was found to be decreased in values from the un-doped titanium to the zirconium-dopant in the order 38.97 nm (un-doped titanium) > 36.65 nm (zirconium-doped titanium) respectively. This could be due to the drag force exerted on the titanium crystal which greatly inhibited the growth rate of titanium dioxide nanoparticle.

This shows a lower number of lattice imperfections. The decreased crystal size was confirmed by the increased values of both the dislocation densities and the micro strain value upon doping as reported by some researchers (Manjula *et al.*, 2015). Smaller particle sizes produce larger surface area for dye anchoring, the reduced crystal sizes promotes light harvesting and elevates charge transfer. The dislocation density (**δ**), was also evaluated. The values obtained showed a gradual increase with the doping mechanism. The implication of the increased dislocation is the displacement of the titanium atoms with the dopant atom confirming successful incorporation of zirconium in the host material. The micro strain (**ε)** was evaluated and the observed values showed very high strain depending on the crystal sizes. It is worth noting that crystals with larger sizes produce more strain since larger molecules exert more suppressing force than smaller particle size. All these observation confirm the introduction of foreign materials into the pure titanium dioxide nanoparticle. The inter-planar distance, d, was estimated from the un-doped titanium sample. A value of 3.38 Å was obtained. The Film thickness decreased from 8.1 μm to 6.1 μm for the un-doped titanium, and zirconium-doped titanium respectively. This change in thickness could be from the method of film deposition adopted during the paste application. Thicker films of solar cells have higher resistance to charge transfer process as the electrons had to travel a longer distance through the material. The thickness of the films together with the bandgap of the synthesized nanoparticles was found to affect electron injection and transfer. Combination of thicker films and big bandgap reduced the rate of electron ejection and charge transfer while the combination of thinner film with smaller bandgap enhanced charge transport and device performance. This was in agreement with some literatures (Domtau *et al.*, 2016; Rajendran *et al.*, 2019) . The estimated values for crystallite sizes, dislocation densities, micro strains and film thicknesses for the synthesized nanoparticles were recorded in Table 1.

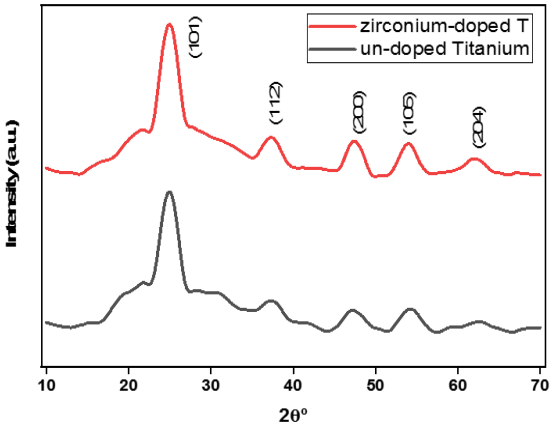


Figure 2: XRD Result of the Synthesized Nanoparticles.

Table 1: Calculated Results from the XRD Studies.

Sample	**2θ (°)**	**FWHM (rad)**	**D (nm)**	**δ ×10^{-3}(nm^{-2})**	**ε × 10^{-3}**	**Film thickness (µm)**
Undoped T	26.36	0.0382	38.97	6.58	40.77	8.1
Zirconium-doped T	24.89	0.0405	36.65	7.44	45.07	6.1

SEM Analysis: Figures 3 depicts the Scanning Electron Microscopy (SEM) morphology in the increasing order of magnification of the synthesized nanoparticles. The results from the sample showed a larger particle size on the un-doped than the doped sample. The SEM morphology of the un-doped has a bigger size particles, highly compacted with little spaces for dye loading. However, after doping, the material underwent significant changes, creating more space and rough surface structure of varying sizes. The increased spacing after doping lead to increased adsorption of dye.

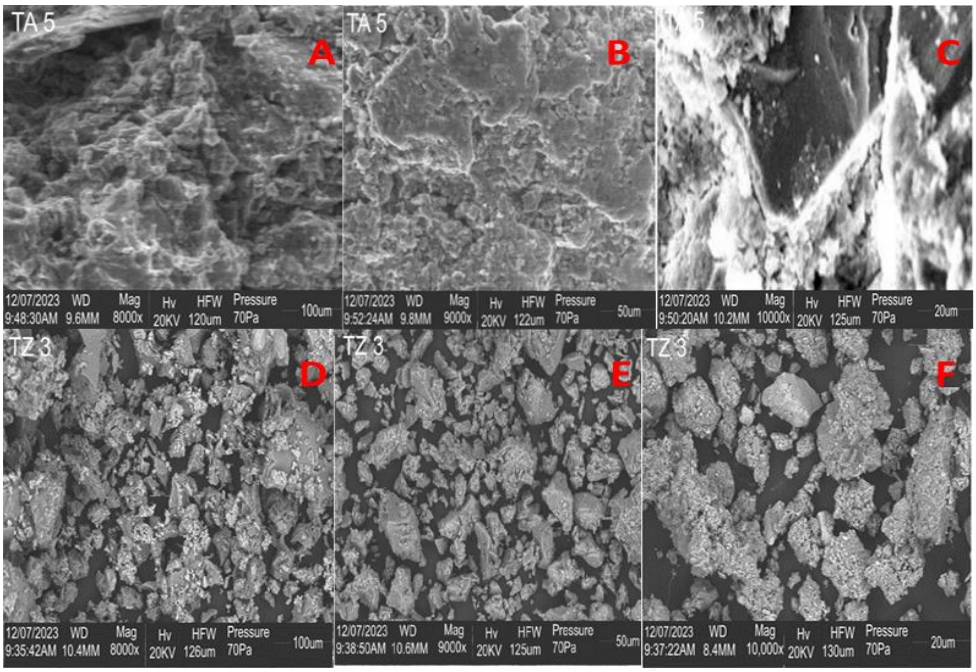


Figure 3: SEM Morphology of the un-doped titanium (a-c) and zirconium-doped titanium (d-f).

Elemental Analysis: The X-ray florescence spectroscopy (XRF) provides information about the chemical elements present in the sample based on the characteristic X-ray emissions from the elements. The XRF spectrum of the synthesized samples are shown in table 2-3. The analysis confirmed the presence of titanium, zirconium, oxygen, hydrogen and carbon in the synthesized samples. However, minor traces of strontium were observed from the samples, this may be ascribed to the contamination from air particles during the synthesis. The XRF results are displayed in table 2 and 3 below. This confirmed the successful synthesis of each of the nanoparticles.

Table 2: The XRF of the un-doped titanium

Element	%	+/- 3σ
Titanium	71.86	0.46
Oxygen	4.12	0.027
Hydrogen	15.77	0.018
Carbon	8.14	0.33
Strontium	0.03	0.005

Table 3: The XRF results of zirconium-doped titanium.

Element	%	+/- 3σ
Titanium	57.67	0.46
Zirconium	5.89	0.015
Nitrogen	7.34	0.013
Oxygen	8.12	0.17
Hydrogen	13.45	0.37
Carbon	7.48	0.012
Strontium	0.05	0.005

Optical Analysis of the Synthesized Nanoparticles: By measuring the absorbance of the synthesized nanoparticle, it is possible to extract the light harvest efficiency. The results of the UV-Vis analysis are presented in figure 3. The un-doped sample transmitted most of the radiation at visible and near Infrared regions. Conversely, the zirconium-doped titanium sample showed relatively high absorbance in both the visible and near infrared regions of the light spectrum. Based on the UV-Vis absorbance spectra, the bandgaps of the synthesized nanoparticles were estimated using the Tauc relation by extrapolating the straight line portion of the curves to a zero absorption coefficient value. The obtained results revealed that the incorporation of the dopant gave rise to a reduction in the bandgap value, indicating a change in the electronic structure of the nanoparticles. Similar reduction in bandgap energy value which promoted electron charge transfer to achieve a more effective ejection of electrons from dye layer to the TiO_2 has been reported (Nguyen & Bark, 2020). The observed reduced bandgap upon doping was in the order; undoped titanium (2.90 eV) > zirconium-doped titanium (2.60 eV). If a bandgap is too high, most daylight photons cannot be absorbed. Alternatively, if bandgap is too low, most photons have much more energy than necessary to excite electrons across the bandgap and the rest of photon energy is wasted. The reduced bandgap was accompanied with red shifts in the absorption peaks, indicating an extended absorption towards the visible region. According to Moss, (1953), the bandgap energy of a material is inversely proportional to its refractive index. As the bandgap energy decreases, the amount of light that is absorbed also increases. The increased absorbance in the visible region from the doped titanium compared to the

un-doped titanium suggests that doping can be used to improve the photoanode to a higher potential for absorption in the visible region, thus rendering them suitable for application in solar cell fabrication. Figures 4–5 displays the UV absorbance spectra and bandgap energies of the synthesized nanoparticles, showing the increase in absorbance in the visible region from the doped sample.

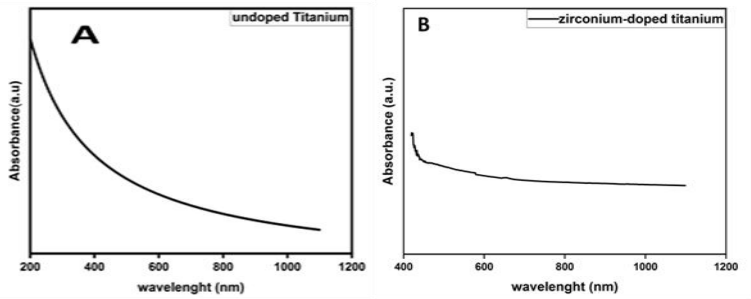


Figure 4: UV-Visible absorbance of the (a) un-doped titanium and (b) zirconium-doped titanium respectively.

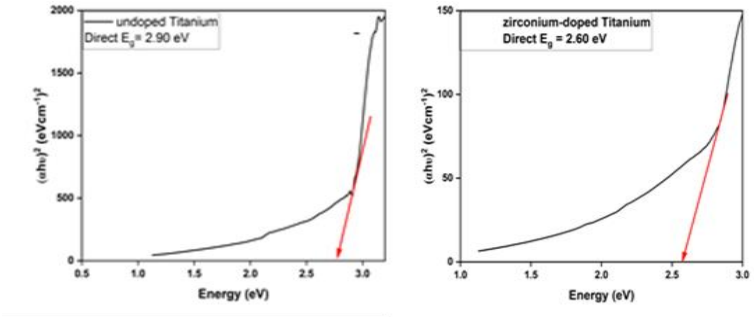


Figure 5: Energy bandgaps of (a) un-doped titanium (b) zirconium-doped titanium respectively.

Optical Absorbance of Dyes: In solar cells, photons are converted into electron. It is therefore desired that as many photons as possible are absorbed. UV-Vis spectroscopy is therefore a commonly used technique to evaluate dyes and their possibility to absorb photons at different wavelengths. The spectral absorbance of the extracted dyes were shown in figure 6. From the graphs, it was observed that the absorbance of the extracted aged dye samples increased from about 30 % in the visible region to about 90 % in the near infra-red region of the electromagnetic spectrum. The absorbance pattern of the dye extract from the un-aged *beta vulgaris* corresponds to the report from Nouairi , *et al.*, (2021) and Mitrevski, *et al.*, (2023). They recorded highest absorption intensity within 530 nm. The aged dye extract from *beta vulgaris* showed a prominent high peak in the UV region at about 300 nm wavelength with gradual increase in the visible and near Infra-red regions, this behavior was evidenced in the photovoltaic properties as the dye tends to absorb efficiently in the visible region. The highest absorption peak of 420 nm was observed from both the aged and un-aged *curcuma longa* dye extracts. This maximum peak absorption was in line with the peaks reported in a researched work (Van Nong *et al.*, 2016). Absorbance is connected to the concentration of a sample, the higher the concentration of a sample, the higher the absorption property. Comparing the absorbance of the dye extracts, the aged dye samples showed outstanding absorbance increase in the visible region. This could be linked to the high concentrations of molecules in the aged dye extracts due to evaporation of the solvents during the long term storage. Thus, the aged dyes have potentials for increased absorption in the visible region and electron ejection, hence can be applied in the fabrication of solar cells.

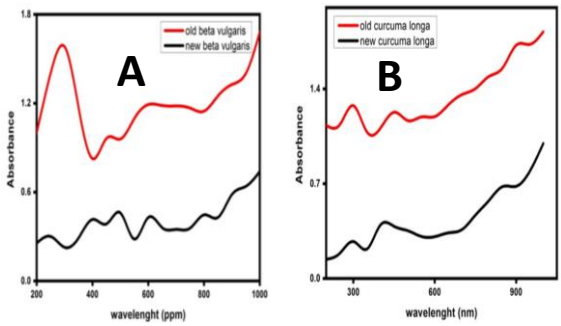


Figure 6: UV Absorbance of (a) beta vulgaris and (b) curcuma longa respectively.

FTIR Analysis of Dye Extracts: The characteristic functionall groups of *beta vulgaris* is shown in figures 7. The transmision bands in *beta vulgaris* indicates that the dye contains characteristic functional groups of O-H alcohol streching vibration at four different wave numbers 3814.879 cm^{-1}, 3688.488 cm^{-1}, 3489.427 cm^{-1} and 3215.961 cm^{-1}, O-H carboxylic acid stretching at 2517.017 cm^{-1}, and 1406.54 cm^{-1} wave numbers. The vibrational strechings of C-H single bonds appeared at 3010.71 cm^{-1}, 2764.44 cm^{-1}, 1297.192 cm^{-1} , 1037.475 cm^{-1} and 886.722 cm^{-1} respectively. A single amino group appeared at wavenumber 3215.961 cm^{-1}. The C=C double bond peaked at same wavenumber with carbonyl group at 1624.46 cm^{-1}. The FTIR spectroscopy of *beta vulgaris* as reported by Nesakumar, *et al.*, (2018) showed same functional groups in *beta vulgaris* dye extract. However, the aged dye extract had more of the hydroxyl functional groups present from both the alcohol and caboxylic acid at 3854.636 cm^{-1}, 3705.33 cm^{-1}, 3577.144 cm^{-1}, 3365.484 cm^{-1}, 3191.564 cm^{-1}, 2790.869 cm^{-1}, 2686.795 cm^{-1} and 2575.566 cm^{-1} respectively. The C─H aromatic methyl stretching peaked at 2938.52 cm^{-1} while its bending appeared at 1389.278 cm^{-1} and 798.524 cm^{-1} respectively. The stetching vibration of the amides was observed at 1318.179 cm^{-1}. The carbonyl from esters was observed at wavenumber 1781.993 cm^{-1} while the conjugate alkenes of C═C bond peaked at 2224.394 cm^{-1}. Clearly, the functional groups present in the aged *beta vulgaris* greatly assisted in light absorption and electron injection into the TiO_2 conduction band for onward charge tranportion onto the back electrode.

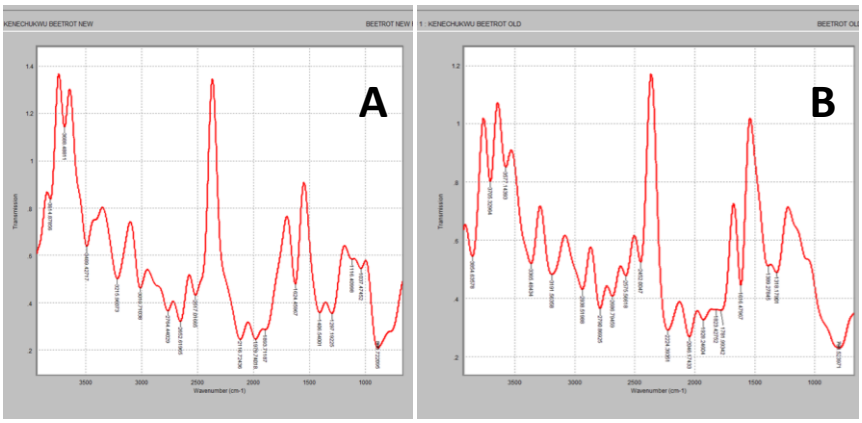


Figure 7: FTIR Transmittance of the Dye Extracts, (a) un-aged beta vulgaris and (b) aged beta vulgaris respectively.

The characteristic functional groups of *curcuma longa* is shown in figure 8. The peaks at 3806.685 cm^{-1}, 3680.207 cm^{-1}, 3414.981 cm^{-1}, 32 58.826 cm^{-1}, 2780.267 cm^{-1} and 2633.162 cm^{-1} indicates the prescence of polyphenols and carboxylic acid in the *curcuma longa* dye extract. An examination of the FTIR spectra by Putri *et al.*, (2019) supports the prescence of

methyl and alkyl groups whose stretching vibration is symmetric and asymetric at IR absorption range between 2500-3000 cm^{-1} wavenumbers. The double bonds of carbonyl (C=O) and C=C with stretching vibration were obsreved at 1627.619 cm^{-1}. Conversly, the O-H alcohol and carboxylic acids occurred at the range 2550-4000 cm^{-1} for the aged *curcuma longa.* IR absorption of aromatic rings and aldehyde bending vibrations occurred between 740-1400 cm^{-1}. These groups enabled efficient electronic coupling between the donor levels of the dye and the acceptor levels of the oxide substrate.

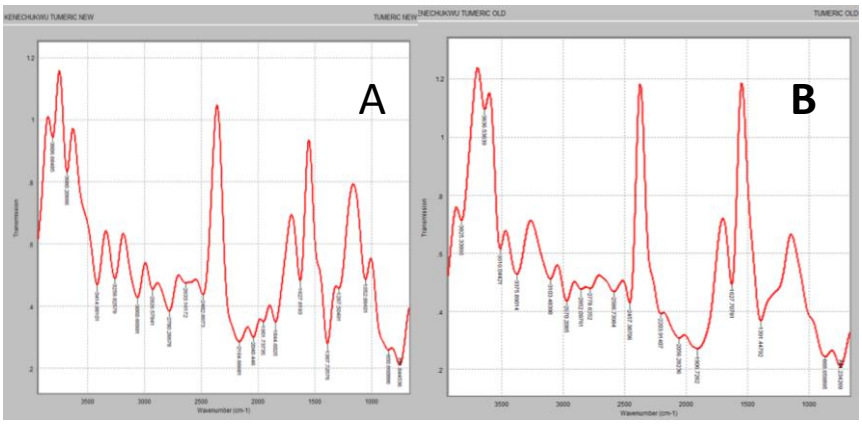


Figure 8. FTIR Transmittance of the Dye Extracts, (a) un-aged *curcuma longa* and (b) aged *curcuma longa* respectively.

DSSC Performance Based on the Un-doped TiO_2: The sensitizer has an influence on the power conversion efficiency of the DSSC and it is important in the determination of the stability of the solar cell. Various solar cells were fabricated using the un-doped titanium sensitized with the extracted dyes. Figure 9 displays the I-V characteristics of the fabricated solar cells. The photovoltaic parameters of the various fabricated solar cells were displayed in table 4. The overview of the results showed that the aged dye extracts have improved power conversion efficiencies compared to the un-aged extracts. The functional groups present in the extracted dyes as evidenced from the infrared studies introduced reactive groups into the bulk material, to form bonds with the metal oxide. This aided the excited electrons mobility to the lowest unoccupied molecular orbital (LUMO) and then into the metal oxide conduction band (CB) with minor loss of energy. Moreover, the concentrated dyes influenced the increased light absorbance. However, the dye extract from the un-aged curcuma longa showed higher PCE than the corresponding aged dye extract. This may be due to the high absorption of the un-aged dye in the visible region due to the presence of more anchoring functional groups as evidenced in the FTIR graph.

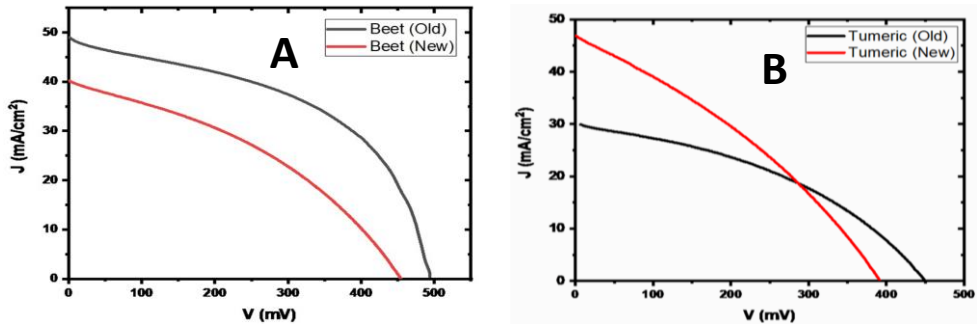


Figure 9. The current-voltage (I-V) characteristics of DSSC fabricated with A (beta vulgaris), and B (curcuma longa).

Table 4: Photovoltaic parameters of various fabricated solar cells

Photoanode	**V_{oc} (V)**	**J_{sc} (Acm^{-2})**	**FF**	**PCE (%)**
Aged turmeric	0.4500	0.030	0.40	0.007
Un-aged turmeric	0.3917	0.047	0.33	0.005
Aged beetroot	0.4958	0.059	0.58	0.012
Un-aged beetroot	0.4543	0.041	0.39	0.006

DSSC Performance based on the Doped TiO_2: The two aged dye extracts, aged *curcuma longa* co-sensitized with the aged *beta vulgaris* was used in the photo sensitization of the zirconium-doped photoanode. Table 5 displays the photovoltaic properties of the fabricated cells while figures 10 and 11 shows the I-V curve and EIS of the samples. The improved photo conversion efficiency recorded from the doped sample could be attributed to the formation of a smaller particle sizes porous upon doping, which gave rise to an increased contact area for dye adsorption, thus increased light absorption in the visible region. Also, the anchoring groups present in the aged sensitizers reacted with the semiconductor's surface and created a chemical bond over which charge transport took place. Moreover, absorbance is directly proportional to the concentration of a material. The higher the concentration of a material, the higher its absorbance because the proportion of light that gets absorbed is affected by the number of molecules that interacts with it. The increased concentration of the dye molecules during the long term storage greatly increased the absorption of the photon energy which increased charge mobility and extraction.

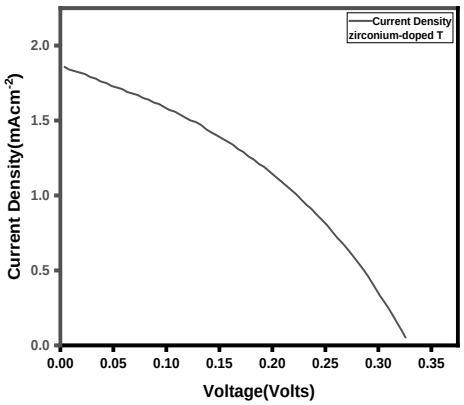


Figure 10: Current density versus Voltage Characteristics of zirconium-doped titanium.

Electro-chemical Impedance Spectroscopy Analysis: The major function of a solar cell is to efficiently generate electrons, charge and voltage. To achieve this, there should be minimal losses and very little resistances for the charge transfer processes in the solar cell. The different components of the solar cell offers resistance within themselves and at the interface between two or more components. Information can be obtained by measuring Electrochemical Impedance Spectroscopy (EIS) of the solar cell from which analysis can be based. Generally, a typical EIS spectrum consists of three semicircles. For a dye sensitized cell, the first resistance that appears is the R_s. This is real, and it is where the measurement point starts in the spectrum. After this, a first semicircle usually diminished, appears, illustrating the resistance at counter electrode interface (R_{ce}). The second semicircle, normally enlarged, is the resistance at the TiO_2/dye surface - electrolyte interface, recombination resistance (R_{rec}) and if a porous counter electrode is used, a last semicircle can appear giving the diffusion resistance

in the counter electrode of the redox couple (R_D). Figure 10 depicts the Nyquist plots of the synthesized nanoparticles. The graphs showed only the series resistance (R_s) and the resistance at the TiO_2/dye surface - electrolyte interface (R_{rec}). The absence of the first semi-circle might be attributed to a very minute resistance from the charge transfer reaction taking place at the counter electrode/ electrolyte interface. The un-doped titanium recorded the least power conversion efficiency. This could be due to the recombination of electrons from the dye, back into the electrolyte generating dark current. The doped sample showed much higher values of the charge transfer resistance at the TiO_2/dye/electrolyte interface (R_{rec}) of 1596.82 Ω (zirconium-doped), the effect of which was demonstrated on the solar cell performance. The improved device performance could be ascribed to low recombination rate of the ejected electrons from the dye into the electrolyte solution. The increased R_{rec} values indicate an improved electron transport on the surface of the photoanode.

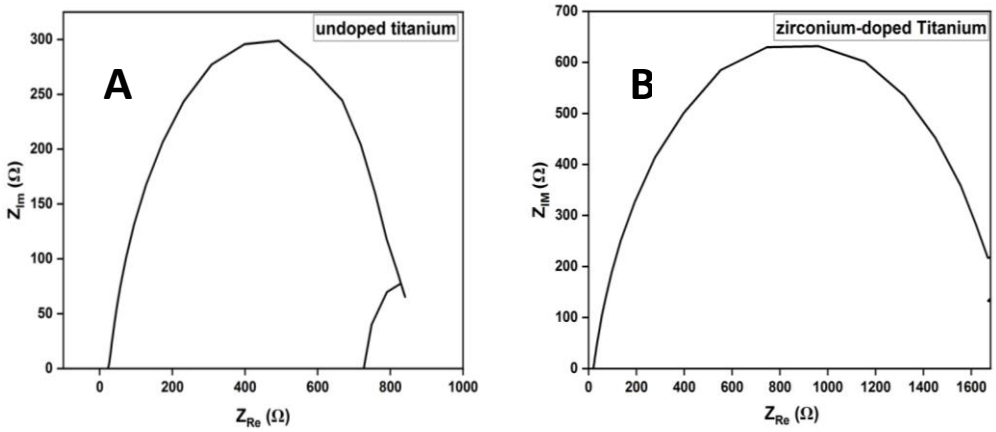


Figure 11: EIS of the (a) un-doped titanium, and (b) zirconium-doped titanium nanoparticles.

Table 5: Photovoltaic and electrochemical parameters of various fabricated solar cells

Photoanode	**J_{sc}(A/cm^2)**	**V_{oc}(V)**	**FF**	**PCE (%)**	**R_s(Ω)**	**R_{rec}(Ω)**
Undoped T	0.059	0.4958	0.58	0.012	23.97	813.87
Zr-doped T	0.186	0.339	0.46	0.788	21.96	1596.82

Conclusion

This study successfully synthesized pristine TiO_2 nanoparticles and doped sample of TiO_2 with zirconium by solvothermal approach for aged natural dye sensitized solar cell applications. Some selected natural dye sources were harvested and natural dye pigments extracted from *beta vulgaris* (beetroot) and *curcuma longa* (turmeric) within the environment. Each of the extracted dye pigments were aged for 14 months before characterizations and fabrications.

The structural, morphological and the optical characterizations of the synthesized photoanodes were obtained. Several solar cells were fabricated using the synthesized photoanodes. Investigation of the photovoltaic properties of the synthesized nanoparticles and the effect of the aged dyes on the performance of the fabricated DSSC device were reported.

The X-ray diffraction (XRD) analysis endorsed the cubic crystal planes of anatase TiO_2 corresponding to the JCPDS card no 21-1272. The zirconium dopant caused a slight left shift

and expansion of the dominant diffraction peak of the (101) plane, this confirms a recognition of an impurity material in the TiO_2 unit cell. The crystal size decreased upon doping as a result of the inhibition of the TiO_2 growth as the dopant exert weights on the host atoms. The reduced crystal size was accompanied with a corresponding increase in dislocation density and microstrain, confirming the effect of the dopant atoms on the host element. The recorded film thickness varied based on the deposition method adopted. The increased thickness reduced charge mobility, as electrons encountered large resistances when traveling the long distance through the large film thickness.

Scanning electron microscopy (SEM) analysis revealed that the undoped TiO_2 nanoparticles had larger crystal sizes and insufficient spaces between the adjacent particles, this affected the dye loading and subsequently the photovoltaic properties. In contrast, the doped sample has more spaces between each adjacent particles as well as rough surfaces with smaller particle sizes. This increased the surface area of the nanoparticles for dye adsorption, and consequently led to higher light absorption.

The energy gap and refractive index of semiconductors represent two fundamental physical aspects that characterize their optical and electronic properties. The energy gap determines the threshold for absorption of photons in semiconductors, and the refractive index in the semiconductor is a measure of its transparency to incident spectral radiation. Also, the bandgap energy of a material is inversely proportional to its refractive index. The UV-Vis analysis of the synthesized nanoparticles showed that the introduction of the dopant reduced the optical bandgap of the TiO_2 semiconducting oxide from 2.90 eV to 2.60 eV, enabling increased light absorption in the visible and near-infrared regions. The enhanced light absorption and electron mobility contributed to the improved performance of the fabricated solar cell as more photons were absorbed from a bigger range of the spectrum.

Furthermore, the study examined the FTIR spectroscopy and the UV-Vis of the dye extracts, this confirmed that all the dye extract had favorable anchoring functional groups which introduced reactive groups into the bulk material, forming bonds with the metal oxide. This aided the excited electrons mobility to the lowest unoccupied molecular orbital (LUMO) into the metal oxide conduction band (CB) without much loss of energy, which significantly narrowed the response spectra of light absorption, photoconductivity, and refractive index of the synthesized nanoparticles. The aged dye extracts generally showed improved properties compared to the un-aged extracts, potentially due to solvent evaporation during the long-term storage, which lead to increased dye concentration. Since absorbance is directly proportional to the concentration of the absorbing species, changes in the dye concentration increased the absorbing strength of the dye pigments. Ageing of the dyes further enhanced their light-absorbing properties, suggesting its potential application in solar cell fabrication.

The EIS analysis provided insights into the series resistance (R_s) and charge transfer resistances (R_{rec}) of the photoanodes. The results indicated a lower values of series resistance from the synthesized nanoparticles. Notably, the zirconium-doped photoanode showed higher value of charge transfer resistance at the photoanode|dye|electrolyte interface (R_{rec}), indicating improved electron transport on their surfaces as more injected electrons were prohibited from recombining with the redox electrolyte. This enhanced the open circuit voltage (V_{oc}) and power conversion efficiency of the solar cell.

These results verifies that the components of a DSSC can be optimized both individually and as a component of a highly interactive assembly. This study highlights the potential of doped

TiO_2 nanoparticles and aged dye extracts for enhancing the performance of DSSCs. The findings contribute to ongoing research efforts aimed at improving the efficiency of NDSSCs and making them a viable option for renewable energy generation.

REFERENCES

Akwolu, R. A., Offiah, S. U., Agbogu, A., Nwakanma, O., Ekechukwu, O. V, Okafor, I. F., & Ugwuoke, P. E. (2023). Comparative study of dyes and effects of purification on selected plants for dye-sensitized solar cells application. *IOP Conference Series: Earth and Environmental Science*, *1178*(1), 12004.

Bartkowiak, A., Korolevych, O., Chiarello, G. L., Makowska-Janusik, M., & Zalas, M. (2021). How can the introduction of Zr^{4+} ions into TiO_2 nanomaterial impact the DSSC photoconversion efficiency? A comprehensive theoretical and experimental consideration. *Materials*, *14*(11), 2955.

Bensaha, R., & Bensouyad, H. (2012). *Synthesis, characterization and properties of zirconium oxide (ZrO_2)-doped titanium oxide (TiO2) thin films obtained via sol-gel process*. IntechOpen.

Bera, S., Sengupta, D., Roy, S., & Mukherjee, K. (2021). Research into dye-sensitized solar cells: a review highlighting progress in India. *Journal of Physics: Energy*, *3*(3), 32013.

Domtau, D. L., Simiyu, J., Ayieta, E. O., Muthoka, B., & Mwabora, J. M. (2016). *Optical and electrical properties dependence on thickness of screen-printed TiO2 thin films*.

Dubey, R. S., Jadkar, S. R., & Bhorde, A. B. (2021). Synthesis and characterization of various doped TiO2 nanocrystals for dye-sensitized solar cells. *ACS Omega*, *6*(5), 3470–3482.

El-Ghamri, H. S., El-Agez, T. M., Taya, S. A., Abdel-Latif, M. S., & Batniji, A. Y. (2014). Dye-sensitized solar cells with natural dyes extracted from plant seeds. *Materials Science-Poland*, *32*, 547–554.

García-Salinas, M. J., & Ariza, M. J. (2019). Optimizing a simple natural dye production method for dye-sensitized solar cells: examples for betalain (bougainvillea and beetroot extracts) and anthocyanin dyes. *Applied Sciences*, *9*(12), 2515.

Geetha, B., & Sumathy, V. J. H. (2013). Extraction of natural dyes from plants. *International Journal of Chemistry and Pharmaceutical Sciences*, *1*(8), 502–509.

Hossain, M. K., Pervez, M. F., Uddin, M. J., Tayyaba, S., Mia, M. N. H., Bashar, M. S., Jewel, M. K. H., Haque, M. A. S., Hakim, M. A., & Khan, M. A. (2018). Influence of natural dye adsorption on the structural, morphological and optical properties of TiO_2 based photoanode of dye-sensitized solar cell. *Mater. Sci*, *36*, 93–101.

Jing, H., Zhu, P., Zheng, X., Zhang, Z., Wang, D., & Li, Y. (2022). Theory-oriented screening and discovery of advanced energy transformation materials in electrocatalysis. *Advanced Powder Materials*, *1*(1), 100013.

Kitiyanan, A., Pavasupree, S., Kato, T., Suzuki, Y., & Yoshikawa, S. (2005). TiO_2-ZrO_2 mixed metal oxide electrode for a dye sensitized solar cell. *Asian Journal on Energy and Environment*, *6*(3), 165–174.

Lai, W.-F., Chao, P.-L., Lin, X.-Y., Chen, Y.-P., Liu, J.-H., Lin, T.-F., Hsu, W.-C., & Huang, C.-Y. (2022). Characteristics of dye-sensitized solar cells with TiO2 stripes. *Materials*, *15*(12), 4212.

Manjula, N., Pugalenthi, M., Nagarethinam, V. S., Usharani, K., & Balu, A. R. (2015). Effect of doping concentration on the structural, morphological, optical and electrical properties of Mn-doped CdO thin films. *Materials Science-Poland*, *33*(4), 774–781.

Mansour, S. A., Farha, A. H., & Kotkata, M. F. (2019). Sol–gel synthesized Co-doped anatase TiO2 nanoparticles: structural, optical, and magnetic characterization. *Journal of Inorganic and Organometallic Polymers and Materials*, *29*(4), 1375–1382.

Mitrevski, J., Pantelić, N. Đ., Dodevska, M. S., Kojić, J. S., Vulić, J. J., Zlatanović, S., Gorjanović, S., Laličić-Petronijević, J., Marjanović, S., & Antić, V. V. (2023). Effect of beetroot powder incorporation on functional properties and shelf life of biscuits. *Foods*, *12*(2), 322.

Mohamed, I. M. A., Dao, V.-D., Barakat, N. A. M., Yasin, A. S., Yousef, A., & Choi, H.-S. (2016). Efficiency enhancement of dye-sensitized solar cells by use of ZrO_2-doped TiO_2 nanofibers photoanode. *Journal of Colloid and Interface Science*, *476*, 9–19.

Moradzaman, M., Mohammadi, M. R., & Nourizadeh, H. (2015). Efficient dye-sensitized solar cells based on CNTs and Zr-doped TiO_2 nanoparticles. *Materials Science in Semiconductor Processing*, *40*, 383–390.

Moss, T. S. (1953). Photoelectromagnetic and photoconductive effects in lead sulphide single crystals. *Proceedings of the Physical Society. Section B*, *66*(12), 993.

Nesakumar, N., Baskar, C., Kesavan, S., Rayappan, J. B. B., & Alwarappan, S. (2018). Analysis of moisture content in beetroot using Fourier transform infrared spectroscopy and by principal component analysis. *Scientific Reports*, *8*(1), 1–10.

Nguyen, T. M. H., & Bark, C. W. (2020). Synthesis of cobalt-doped TiO_2 based on metal–organic frameworks as an effective electron transport material in perovskite solar cells. *ACS Omega*, *5*(5), 2280–2286.

Nirmala, M., Sahana, S., Iswarya, B., Maruvarasi, K., Jenita, A. A., & Kavitha, B. (2020). Fabrication of dye sensitized solar cell based on natural photosensitizers. *World Scientific News*, *149*, 128–139.

Nouairi, M. E.-A., Freha, M., & Bellil, A. (2021). Study by absorption and emission spectrophotometry of the efficiency of the binary mixture (Ethanol-Water) on the extraction of betanin from red beetroot. *Spectrochimica Acta Part A: Molecular and Biomolecular Spectroscopy*, *260*, 119939.

Offiah, S. U., Agbo, S. N., Ezema, C. G., Ugwuoke, P. E., Ekwealor, A. B. C., Agbogu, A. N. C., Ezekoye, B. A., & Ezema, F. I. (2021). Enhancement of the performance of ZnO based natural dye sensitized solar cells via PVA morphology controlled nanorods. *IOP Conference Series: Earth and Environmental Science*, *730*(1), 12033.

Onah, E. O., Offiah, S. U., Chime, U. K., Whyte, G. M., Obodo, R. M., Ekechukwu, O. V, Ahmad, I., Ugwuoke, P. E., & Ezema, F. I. (2020). Comparative photo-response performances of dye sensitized solar cells using dyes from selected plants. *Surfaces and Interfaces*, *20*, 100619.

Pastuszak, J., & Węgierek, P. (2022). Photovoltaic cell generations and current research directions for their development. *Materials*, *15*(16), 5542.

Pawar, K. S., Baviskar, P. K., Inamuddin, Nadaf, A. B., Salunke-Gawali, S., & Pathan, H. M. (2019). Layer-by-layer deposition of TiO 2–ZrO 2 electrode sensitized with Pandan leaves: natural dye-sensitized solar cell. *Materials for Renewable and Sustainable Energy*, *8*, 1–9.

Putri, A. S., Octavianty, T. D., Wahyudi, N. T., & Safitri, A. (2019). Preparation of Nanoparticles from Curcuma longa L. and Cosmos caudatus Extracts. *Journal of Physics: Conference*

Series, *1374*(1), 12027.

Rosana, N. T. M., & Amarnath, D. J. (2014). Dye Sensitized Solar Cells for the Transformation of Solar Radiation into Electricity. *Indian Journal of Applied Research*, *4*(6).

Shelke, R. S., Thombre, S. B., & Patrikar, S. R. (2013). Status and perspectives of dyes used in dye sensitized solar cells. *International Journal of Renewable Energy Resources*, *3*(2), 54–61.

Syafinar, R., Gomesh, N., Irwanto, M., Fareq, M., & Irwan, Y. M. (2015). Chlorophyll pigments as nature based dye for dye-sensitized solar cell (DSSC). *Energy Procedia*, *79*, 896–902.

Taya, S. A., El-Agez, T. M., El-Ghamri, H. S., & Abdel-Latif, M. S. (2013). Dye-sensitized solar cells using fresh and dried natural dyes. *International Journal of Materials Science and Applications*, *2*(2), 37–42.

Tomar, L. J., Bhatt, P. J., Desai, R. K., Chakrabarty, B. S., & Panchal, C. J. (2016). Improved conversion efficiency of dye sensitized solar cell using Zn doped TiO_2-ZrO_2 nanocomposite. *AIP Conference Proceedings*, *1731*(1).

Van Nong, H., Hung, L. X., Thang, P. N., Chinh, V. D., Vu, L. Van, Dung, P. T., Van Trung, T., & Nga, P. T. (2016). Fabrication and vibration characterization of curcumin extracted from turmeric (Curcuma longa) rhizomes of the northern Vietnam. *Springerplus*, *5*, 1–9.

Waghmare, M. A., Beedri, N. I., Ubale, A. U., & Pathan, H. M. (2019). Fabrication and characterization of rose bengal sensitized binary TiO_2-ZrO_2 oxides photo-electrode based dye-sensitized solar cell. *Engineered Science*, *6*(4), 36–43.

Widhiyanuriyawan, D., Harsito, S. D. W. I. P., & Suyitno, Z. A. (2022). Natural dye sensitizers mixture of curcumin, chlorophyll, and anthocyanin for dye-sensitized solar cells. *Journal of Engineering Science and Technology*, *17*(6), 3755–3765.

Win, S. Y., Win, T. T., Maung, Y. M., Soe, K. K. K., Kyaw, T. T., Tan, C. K., Rajalingam, S., & Oo, Z. (2015). Synthesis of nanoparticalbased binary oxide electrode TiO_2–ZrO_2 with carrot-derived natural dye extract for dye sensitized solar cell (DSSC) application. *Pertanika J. Sci. Technol*, *23*(1), 119–125.

Zhang, D., Lanier, S. M., Downing, J. A., Avent, J. L., Lum, J., & McHale, J. L. (2008). Betalain pigments for dye-sensitized solar cells. *Journal of Photochemistry and Photobiology A: Chemistry*, *195*(1), 72–80.